Clim Dyn
DOI 10.1007/s00382-010-0959-z

Role of the ocean in controlling atmospheric CO_2 concentration in the course of global glaciations

Akira Oka · Eiichi Tajika · Ayako Abe-Ouchi · Keiko Kubota

Received: 15 February 2010 / Accepted: 24 November 2010

Abstract Responses of ocean circulation and ocean carbon cycle in the course of a global glaciation from the present Earth conditions are investigated by using a coupled climate-biogeochemical model. We investigate steady states of the climate system under colder conditions induced by a reduction of solar constant from the present condition. A globally ice-covered solution is obtained under the solar constant of 92.2% of the present value. We found that because almost all of sea water reaches the frozen point, the ocean stratification is maintained not by temperature but by salinity just before the global glaciation (at the solar constant of 92.3%). It is demonstrated that the ocean circulation is driven not by the surface cooling but by the surface freshwater forcing associated with formation and melting of sea ice. As a result, the deep ocean is ventilated exclusively by deep water formation in southern high latitudes where sea ice production takes place much more massively than northern high latitudes. We also found that atmospheric CO_2 concentration decreases through the ocean carbon cycle. This reduction is explained primarily by an increase of solubility of CO_2 due to a decrease of sea surface temperature, whereas the export production weakens by 30% just before the global glaciation. In order to investigate the conditions for the atmospheric CO_2 reduction to cause global glaciations, we also conduct a series of simulations in which the total amount of carbon in the atmosphere–ocean system is reduced from the present condition. Under the present solar constant, the results show that the global glaciation takes place when the total carbon decreases to be 70% of the present-day value. Just before the glaciation, weathering rate becomes very small (almost 10% of the present value) and the organic carbon burial declines due to weakened biological productivity. Therefore, outgoing carbon flux from the atmosphere–ocean system significantly decreases. This suggests the atmosphere–ocean system has strong negative feedback loops against decline of the total carbon content. The results obtained here imply that some processes outside the atmosphere–ocean feedback loops may be required to cause global glaciations.

Keywords Ocean carbon cycle · Global glaciation · Climate model

1 Introduction

Paleomagnetic studies of glaciogenic deposits indicate that ice sheets reached the Equator during the Neoproterozoic (e.g., Evans 2000). It may be interpreted as the results of the "snowball earth" event where the entire earth was glaciated at that time. Numerical studies using an energy balance model (EBM) have suggested the possibility of a globally ice-covered state (e.g., Budyko 1969; Sellers 1969; North 1981). These studies indicate that stable climate states can be classified into three distinct branches: an ice-free branch, a partially ice-covered branch, and a globally ice-covered branch. They demonstrate that the partially ice-covered branch disappears when a solar constant or atmospheric CO_2 concentration falls below a critical level.

A. Oka (✉) · A. Abe-Ouchi
Atmosphere and Ocean Research Institute, University of Tokyo,
5-1-5 Kashiwanoha, Kashiwa, Chiba 277-8568, Japan
e-mail: akira@aori.u-tokyo.ac.jp

E. Tajika · K. Kubota
Department of Earth and Planetary Science,
Graduate School of Science, University of Tokyo,
7-3-1 Hongo, Bunkyo-ku, Tokyo 113-0033, Japan

Published online: 19 December 2010

The solar constant is believed to increase with time on geological time scale. According to the standard model of solar evolution (Gough 1981), the solar constant is estimated to be 94% of the present-day value during the Neoproterozoic. The above-mentioned EBM simulations and other numerical studies indicate that this lower solar constant alone cannot have initiated the global glaciation (e.g., Tajika 2003). The most promising process which triggers the global glaciation is reduction of the concentration of atmospheric greenhouse gases. Recent numerical studies focus on the critical level toward the global glaciation by using more sophisticated climate models. Jenkins and Smith (1999) used an atmospheric general circulation model (AGCM) coupled with a slab ocean model. Under 94% of the present-day solar constant, they obtain a globally ice-covered state at atmospheric CO_2 pressure (CO_2) level of 100 ppm. Since EBM simulation by Crowley and Baum (1993) do not result in a globally ice-covered state even at pCO_2 level of 40 ppm in the same situation, they speculate that difference in representation of atmospheric heat transport or other physical processes may affect the critical level. Chandler and Sohl (2000) use an AGCM coupled with a slab ocean in the same way as Jenkins and Smith (1999). Contrary to Jenkins and Smith (1999), they do not obtain a globally ice-covered state but a partially ice-covered state with 30% of ice-free area. Hyde et al. (2000) conduct simulations with a dynamical ice-sheet model and demonstrate that the model results in a globally ice-covered state more easily by inclusion of ice-sheet dynamics. They also obtained a "soft-snowball earth" state where ice-free ocean exists near the equator. They speculated that this solution is more advantageous than the "hard-snowball" earth (global glaciation) solution for explaining survival of multicellular organisms. By prescribing the ice-sheet distribution obtained in Hyde et al. (2000) and using an AGCM coupled with a slab ocean model, Baum and Crowley (2001) investigates threshold level of pCO_2 separating hard-snowball and soft-snowball earth solutions. They obtain a hard-snowball earth solution under 0.5 and 1.0 times the present-day pCO_2 level and a soft-snowball earth solution under 2.0 and 2.5 times level of the present-day pCO_2. Recently, the importance of sea ice dynamics is also pointed out (Lewis et al. 2004; 2007). Lewis et al. (2007) suggests that a soft-snowball earth solution is difficult to be obtained when dynamics of sea ice are included in the model. Poulsen et al. (2001, 2002) use a coupled atmosphere and ocean general circulation model and investigated the role of ocean dynamics on a globally ice-covered solution. However, since their integration time is shorter than the time scale of ocean deep circulation and the number of simulations is restricted, the critical level of pCO_2 is difficult to be referenced from their results. By use of a coupled ocean–atmosphere model of intermediate complexity, Donnadieu et al. (2004a) demonstrate that the critical level is affected by continental distribution where a globally ice-covered state is obtained at 89 and 149 ppm of pCO_2 in the supercontinent case and in the dislocated configuration, respectively.

Besides identifying the critical level of pCO_2, it is still in a debate how the reduction of pCO_2 takes place during the Neoproterozoic. Several possibilities have been raised by previous studies. For example, an increase in the organic carbon burial may have decreased pCO_2 and caused the global glaciation (Kaufman et al. 1997; Hoffman et al. 1998). In addition to the increased rate of organic carbon burial, Tajika (2004) shows that the reduction of volcanic-metamorphic activities would have been required to cause the global glaciations. On the other hand, by using a simple climate-carbon coupled model, Donnadieu et al. (2004b) argues that the decrease of pCO_2 could have been caused by an increase in silicate weathering, owing to an increase in river runoff and emplacement of food basalt through the break-up of the supercontinent Rodinia. On the contrary, by focusing on the dependency of remineralization rate of massive pool of dissolved organic carbon on oxygen concentration, Peltier et al. (2007) points out that drawdown of atmospheric oxygen into the ocean in colder climate leads to the increased rate of remineralization and acts as negative feedback toward a global glaciation.

Changes in biological carbon pump and burial rate of organic carbon have been raised as a possible mechanism for decreasing pCO_2 as described above. The role of the ocean on determining the critical level of pCO_2 has been investigated by using an ocean general circulation model (OGCM) in the previous studies (Poulsen et al. 2001, 2002). On the other hand, the carbon cycle in the ocean has not been explicitly simulated so far in spite of its importance on controlling pCO_2. It is therefore important to discuss the role of ocean not only in determining the critical level of pCO_2 but also in controlling pCO_2 itself. The mechanism controlling pCO_2 by the ocean carbon cycle can be categorized into two processes. The first process comes from redistribution of carbon between the ocean and atmosphere while the total carbon amount in the atmosphere and ocean system is unchanged. The other process comes from changes in the total carbon amount in the atmosphere and ocean system induced by changes in carbon flux inflowing into and outflowing from the atmosphere–ocean system. Changes in solubility of CO_2 into the ocean associated with SST and SSS changes are categorized into the first process. Changes in the ocean circulation and biological pump may modify surface concentration of dissolved inorganic carbon and alkalinity in the ocean, which affects the oceanic pCO_2. They are also categorized into the first process. On the other hand, changes in the

accumulation rate of carbon at seafloor sediments and input of volcanic CO_2 lead to changes in the total carbon amount in the ocean and atmosphere system. They are categorized into the second process.

In this study, the physical and biogeochemical changes in the ocean in the course of global glaciations from the present Earth conditions are investigated by using a coupled climate-biogeochemical cycle model. We conduct two series of simulations. In the first series of simulations, the first process mentioned above is evaluated by reducing the solar constant from the present value to that resulting in a globally ice-covered state. In these simulations, while the model explicitly simulates three dimensional ocean dynamics and carbon cycles, the total amount of the carbon in the atmosphere and ocean is assumed to be constant. In the second series of simulations, the above-mentioned second process is discussed; we conduct simulations under various values of the total carbon amount and evaluate how atmospheric pCO_2 changes when the total carbon amount in the ocean and atmosphere system is modified. We also investigate how the carbon flux inflowing into and outflowing from the ocean can be changed via feedback processes of the atmosphere–ocean system in a very cold climate state. It is the first attempt to evaluate effects of ocean carbon cycle in the course of global glaciations by explicitly calculating three dimensional ocean dynamics and biogeochemical cycles. We systematically conduct series of simulations with various values of the solar constant and the total carbon amount. Owing to these treatments, we can clearly investigate what happens in the ocean carbon cycle when the present climate gradually shifts to a very cold climate and discuss which process is important for controlling the atmospheric pCO_2 therein. We evaluate the role of the ocean in controlling atmospheric pCO_2 in the course of global glaciations in more sophisticated and systematic way than the previous studies.

The model used in this study is developed so that the present climate may be reproduced well (Oka et al. 2001). Therefore, we use the well-known present climate condition as a control simulation in this study. We then investigate how the atmosphere–ocean system changes from the present climate to a globally-glaciated climate. We can clearly discuss how normal (present) climate will change in the course of global glaciations. Based on the results obtained from the above-mentioned experimental design, we discuss common and different aspects between our simulations and the snowball earth events during the Neoproterozoic. We may be able to simulate the Neoproterozoic snowball earth events directly with a reconstructed land-sea distribution and the estimated solar constant for that period. We however do not investigate directly the Neoproterozoic snowball earth events in this study.

The paper is organized as follows. In Sect. 2, the model used in this study is explained. Experimental design of numerical simulations is described in Sect. 3. The results of the simulations are shown in Sect. 4. In Sect. 5, we discuss processes controlling the total carbon amount of the atmosphere–ocean system. The summary of our study is given in Sect. 6.

2 Model

The physical model used in this study is named as MIROC-lite. The earlier version of MIROC-lite is described in Oka et al. (2001). The model consists of an atmospheric energy and moisture balance model, a one-layer bucket land model, an OGCM, and a dynamical sea-ice model. The model is coupled with an ocean biogeochemical model in this study. These models are briefly described in this section. References required for further information are also stated therein. As for the atmosphere, land, and ocean biogeochemical models, the detailed descriptions are given in Appendix. In all the model components, the model domain is global and has 90×45 grid points in horizontal directions. There are 35 vertical layers for the ocean model.

2.1 The ocean model

The OGCM used in this study is Center for Climate System Research (CCSR) Ocean Component Model (COCO) version 4.0 (Hasumi 2006) which constitutes an oceanic part of MIROC (MIROC is a fully coupled general circulation model; K-1 model developers 2004). This is a free surface model which explicitly predicts changes in sea surface height by the method of Killworth et al. (2003). Isopycnal diffusion (Cox 1987), isopycnal thickness diffusion (Gent et al. 1995), and surface mixed layer (Noh and Kim 1999) parameterizations are applied in the model. Sea surface elevation, tracers, and velocity components are filtered in the zonal direction in the Arctic Ocean to use a time step longer than the limit of the CFL condition in the Arctic Ocean.

2.2 The sea ice model

The sea ice model comprises both thermodynamic and dynamic components. The thermodynamic part is the zero layer model of Semtner (1976). In the dynamic part, internal ice stress is formulated by the elastic–viscous–plastic rheology (Hunke and Dukowicz 1997). The model predicts ice thickness, areal fraction, and ice velocity in each grid. The sea ice salinity is assumed to be constant (3 psu) in this study. The COCO coupled to this sea ice model has been used for sensitivity studies of global thermohaline

circulation (e.g., Oka and Hasumi 2004; Komuro and Hasumi 2003) and other related studies (e.g., Tanaka and Hasumi 2008; Watanabe and Hasumi 2009).

2.3 The atmosphere and land models

The atmospheric model is the energy and moisture balance model where air temperature and air specific humidity are predicted as prognostic variables and the wind is diagnosed from meridional gradient of air temperature as described in Oka et al. (2001). In this study, the model also includes a simple bucket model in which ground temperature, wetness, and snow amount are explicitly calculated. The detailed description is given in Appendix.

2.4 The ocean biogeochemical cycle model

The model is based on Yamanaka and Tajika (1996) where phosphate, dissolved carbon, and alkalinity are calculated as prognostic variables. The oceanic surface pCO_2 is derived from surface temperature, salinity, dissolved carbon, and alkalinity. The model includes a well-mixed atmosphere box in which atmospheric CO_2 concentration is calculated from gas exchange between the ocean and the atmosphere. Photosynthesis takes place above depth of 50 m, where the export production is diagnosed from in-situ phosphate concentration and light factor which is simple function of latitude. The production of calcium carbonate is proportional to the export production, and its ratio called "rain ratio" is set to be 0.08 as a globally constant value. The profile of vertical flux of particulate organic matter is represented by a power law obtained from sediment traps (Martin et al. 1987). The profile of calcium carbonate is taken from the control case of Yamanaka and Tajika (1996). The detailed model description is given in Appendix.

3 Experimental design

We assume the present-day boundary conditions except for the solar constant and the total carbon amount in the atmosphere–ocean system for all the simulations in this study, including land-sea distribution, sea-floor topography, and ocean chemistry. The control case is therefore the reproduction of the Earth at present. Then, we conduct a series of simulation with different values of the solar constant or the total carbon content in the atmosphere–ocean system to investigate changes in climate, ocean dynamics, and ocean carbon cycle from the control case. This is because we know the present Earth conditions much better than those of the past, and try to know how the Earth falls into global glaciations from the present conditions. In this respect, we do not aim at investigating the cause of the Neoproterozoic snowball Earth events directly, although we will discuss it based on the results of this study.

As the first experiment, we conduct "S-series" simulations. In this experiment, we carry out simulations by changing a value of the solar constant. The purpose of this experiment is to describe changes in ocean physical and biogeochemical states, and to investigate effects of the ocean carbon cycle on the atmospheric pCO_2 in the course of global glaciations. In order to evaluate physical and biogeochemical responses of the ocean individually, the changes in the ocean carbon cycle are assumed to have no feedback effects on the climate in this experiment (i.e., the outgoing longwave radiation is not affected by changes in the atmospheric pCO_2).

In the second experiment, we conduct "C-series simulations". In this experiment, while the solar constant does not change, we reduce the total amount of carbon contained in the atmosphere–ocean system. The globally-integrated value of the total amount of carbon in the atmosphere–ocean system is conserved at a value given as an initial condition. Therefore, the experiment is conducted from various initial conditions with different amount of the total carbon under both 100 and 94% of the present-day solar constant. The aim of this experiment is to investigate the critical level of pCO_2 in our model and evaluate how much total carbon in the atmosphere–ocean system is required for the reduction of pCO_2 to cause a global glaciation. We also discuss feedback processes of the ocean carbon cycle against the reduction of the total carbon amount in the atmosphere–ocean system.

4 Result

4.1 The S-series experiment

In all the simulations of this experiment, the model is integrated for 2000 years from the present climatology: temperature and salinity from Steele et al. (2001), phosphate from Conkright et al. (2002), and dissolved carbon and alkalinity from Key et al. (2004). The average over the last 100 years of the integration is shown here.

4.1.1 Physical response

The globally averaged sea ice concentration and air temperature against value of the solar constant are plotted in Fig. 1a, b, respectively. As in the previous studies using EBM, the model simulates partially ice-covered states (between 100 and 92.3% of the present-day solar constant) and globally ice-covered states (<92.3% of the present-day solar constant). Between 100 and 92.3% of the present-day

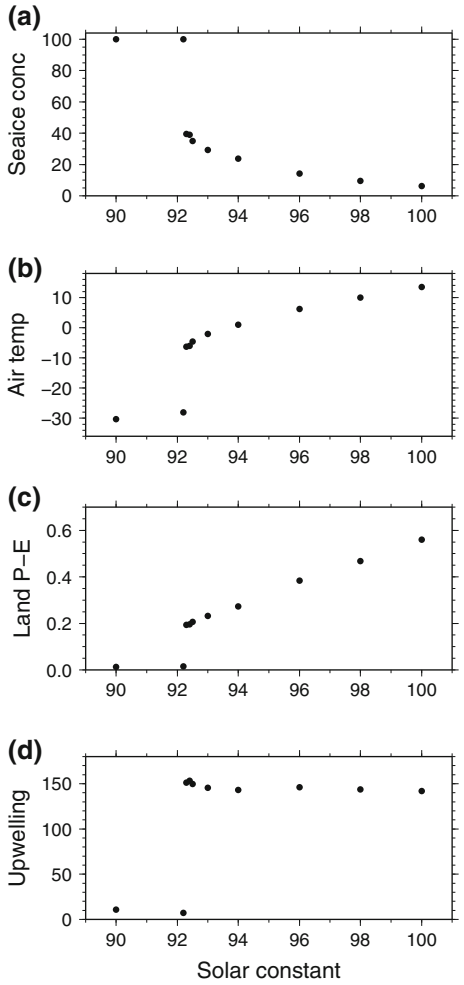

Fig. 1 The globally averaged (**a**) sea ice concentration (%), (**b**) air temperature (°C), globally integrated (**c**) precipitation minus evaporation over land (Sv), and (**d**) ocean upwelling (Sv) plotted against solar constant (%) in S-series simulations. The solar constant is shown by relative value to Control

solar constant, air temperature gradually decreases and ice-covered area spreads toward low latitudes. At 92.2% of the solar constant, the result suddenly shifts to a globally ice-covered state and air temperature drops below freezing point over the globe. Since the atmospheric vapor content changes exponentially with temperature, the hydrological cycle significantly weakens in colder climate (Fig. 1c). The Ekman upwelling, which is important for the biological production, becomes almost zero in a globally ice-covered state since sea ice prevents wind stress from driving the ocean (Fig. 1d). In partially ice-covered states, the Ekman upwelling becomes slightly stronger for colder climate because of larger meridional gradient of air temperature.

In Fig. 2, we focus on differences between a state under the present-day solar constant (Control), a state just before a global glaciation (S92.3), and a globally ice-covered state (S92.2). In Control, the sea ice exists only at high latitudes as in the present climate (Fig. 2a). On the other hand, the ice-free area is limited between 15°S ∼ 15°N in S92.3, and no ice-free area is found in S93.2. The significant meridional gradient of air temperature is observed in all the simulations (Fig. 2b), whereas the SST gradient vanishes over the ice-covered area since SST cannot become below the freezing point (Fig. 2c). The differences in SSS among the simulations (Fig. 2d) are not similar to those in SST, which is closely linked to the ocean circulation as described below.

Figure 3 displays the global ocean circulation in Control and S92.3. In Control, the deep ocean circulation originates from northern and southern high latitudes, associated with the formation of North Atlantic Deep Water (NADW) and Antarctic Bottom Water (AABW), respectively. On the other hand, there is no NADW formation and the deep ocean circulation originates exclusively from southern high latitudes in S92.3. In Control, ocean stratification is determined mainly by temperature, and tight lower thermocline develops above 1,000 m and vertical salinity gradient is of secondary importance except at high latitudes (Fig. 4). On the other hand, in S92.3, water at the near-freezing point occupies almost the entire ocean and water above the freezing point is found only at very shallow depth over ice-free region. Then, contrary to Control, vertical stratification is kept exclusively by vertical salinity gradient in S92.3. Such salinity distribution relates to massive sea ice formation in high latitudes and melting in low latitudes (Fig. 5), which is maintained by wind-induced sea ice transport toward low latitudes. This sea-ice freshwater cycle is also found in Control and enormously intensified in S92.3. Because the surface heat flux almost vanishes by an insulation effect of sea ice, the thermohaline circulation is driven purely by the surface freshwater forcing in S92.3. Such salinity-driven thermohaline circulation is also reported by previous modeling studies (e.g., Hasumi and Suginohara 1995). Since there is less lands in the Southern hemisphere than the Northern hemisphere at the present, sea ice is transported toward low latitudes more efficiently and amplitude of net sea ice production becomes larger in the Southern hemisphere (Fig. 5). This explains why the deep water formation takes place in southern high latitudes in S92.3 (Fig. 3b). As for a globally ice-covered state (i.e., S92.2), there is no ice-free area and sea ice is not easily transported due to internal stress of sea ice. Therefore, there is almost no heat flux and small freshwater flux at sea surface. This leads to a nearly static state with almost uniform temperature and weak salinity stratification (figures not shown). We should note that more careful treatment of sea ice and ocean should be required when sea ice thickness enormously increases (e.g., Goodman and Pierrehumbert 2003). However, we discuss

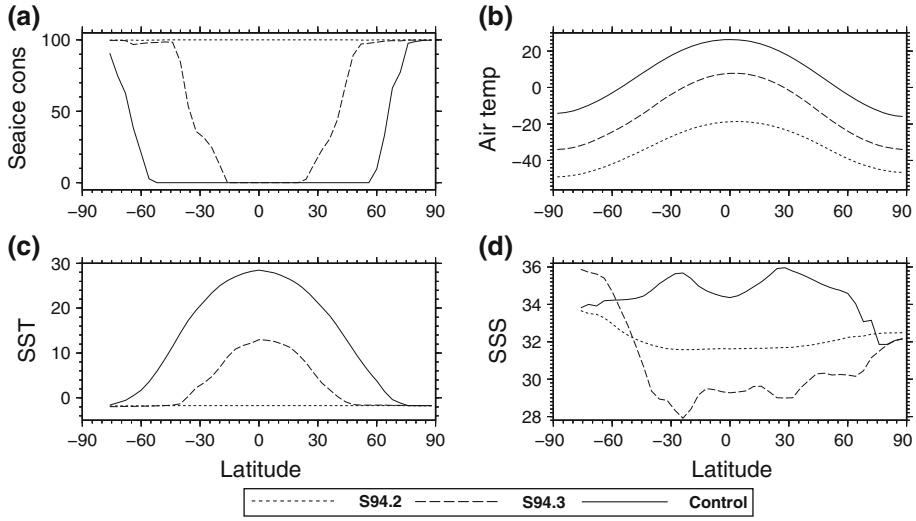

Fig. 2 The zonally averaged (**a**) sea ice concentration (%), (**b**) air temperature (°C), (**c**) SST (°C), and (**d**) SSS (psu). The *solid*, *broken*, and *dotted lines* are for Control, S92.3, and S92.2, respectively

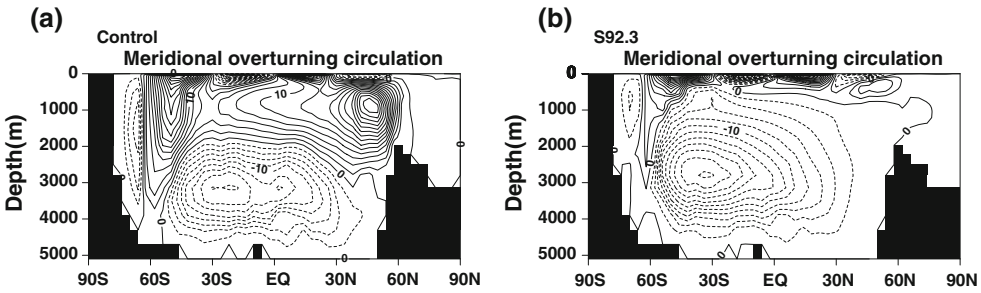

Fig. 3 The global meridional overturning circulation in (**a**) Control and (**b**) S92.3. The contour interval is 1 Sv

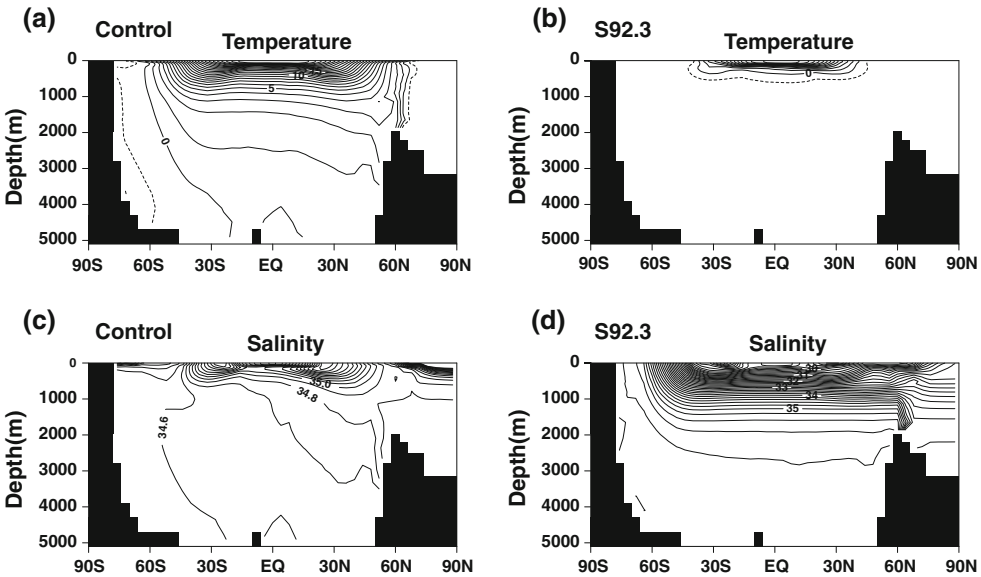

Fig. 4 The zonally averaged ocean temperature (*top*) and salinity (*bottom*), (**a**, **c**) in Control, and (**b**, **d**) in S92.3. The contour intervals are 1°C in (**a**) and (**b**), 0.1 psu in (**c**), and 0.2 psu in (**d**)

here the characteristic behaviors of the Earth system through the climate change from the present state to a globally ice-covered state, and, at least, the initial behaviors could be largely captured by the present treatment of sea ice. We believe that the results obtained here are robust responses of the ocean in the course of global glaciations from the present Earth conditions.

4.1.2 Biogeochemical response

Figure 6a plots the atmospheric pCO_2 against the solar constant in S-series simulations. As the solar constant becomes smaller, the atmospheric CO_2 concentration decreases from Control to S92.3. The atmospheric pCO_2 variation arises from change in oceanic pCO_2 or that in

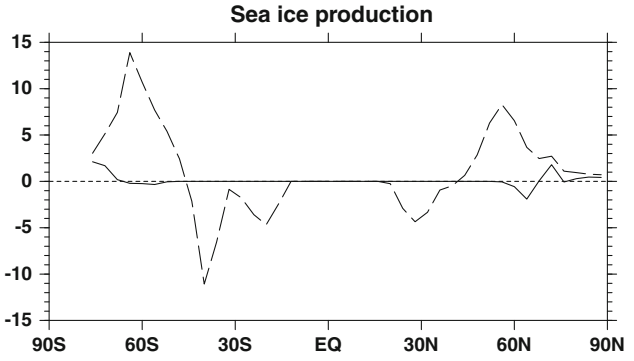

Fig. 5 The zonally averaged net sea ice production (i.e., forming minus melting). *Solid* and *dashed lines* are for Control and S92.3, respectively. Negative value means net melting takes place. Unit is 10^{-6} cm/s

pCO_2 difference between the atmosphere and the ocean. In our results, the changes in atmospheric pCO_2 are explained mainly by changes in oceanic pCO_2 (Fig. 6a, b). Since the oceanic pCO_2 depends on SST, SSS, dissolved inorganic carbon, and alkalinity (e.g., Sarmient and Gruber 2006), combined effects of their changes determine the oceanic pCO_2 variation. In order to investigate which effect is the most important for the changes in pCO_2, we evaluated the effects of SST, SSS, dissolved inorganic carbon (*DIC*), and alkalinity (*ALK*) changes separately (Fig. 6b). In this evaluation, the effects of SST ($pCO_2(SST)$), SSS ($pCO_2(SSS)$), and concentration of dissolved carbon and alkalinity ($pCO_2(DIC + ALK)$) on pCO_2 are in the following equations;

$$pCO_2(SST) = f(SST_{ref} + \Delta SST, SSS_{ref}, DIC_{ref}, ALK_{ref}), \quad (1)$$

$$pCO_2(SSS) = f(SST_{ref}, SSS_{ref} + \Delta SSS, DIC_{ref}, ALK_{ref}), \quad (2)$$

$$pCO_2(DIC + ALK) = f(SST_{ref}, SSS_{ref}, DIC_{ref} + \Delta DIC, ALK_{ref} + \Delta ALK), \quad (3)$$

where the subscript *ref* indicates reference value (taken from Control experiment), Δ represents difference from Control, and f is a symbolical function of oceanic carbon chemistry (see Eq. 56). They are numerically calculated by using *SST*, *SSS*, *DIC*, and *ALK* in each simulation. The figure suggests that pCO_2 changes are primarily determined by SST changes; colder SST leads to high CO_2 solubility of the ocean. Decline of SSS, caused by sea ice melting over ice-free region, slightly contributes to a decrease of pCO_2. On the other hand, changes in concentration of dissolved carbon and alkalinity slightly increase CO_2 pressure, which is described in detail below. Concentrations of dissolved carbon and alkalinity are determined under the balance among the biological pump, ocean circulation, and diluting/condensation by surface freshwater flux (and gas exchange with the atmosphere for dissolved carbon).

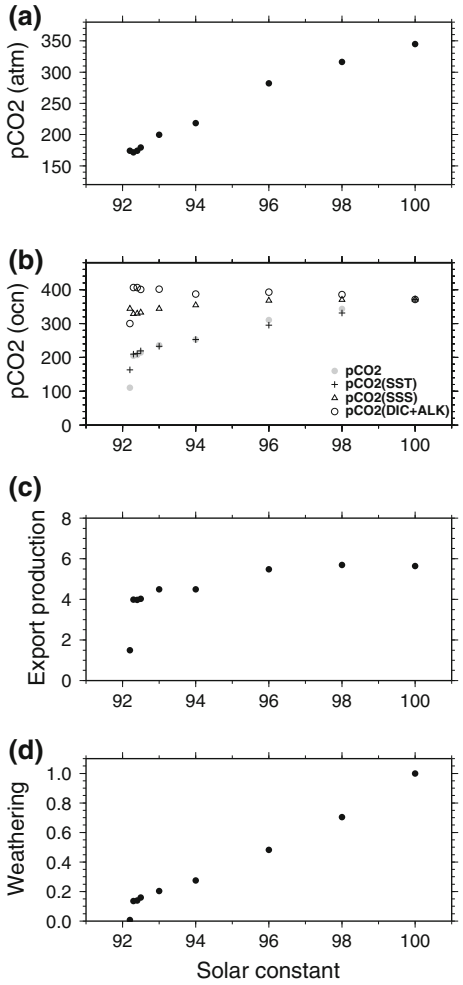

Fig. 6 The globally averaged (**a**) atmospheric CO_2 pressure (ppm), (**b**) CO_2 pressure of surface ocean (ppm), (**c**) global export production (GtC/yr), and (**d**) estimated weathering rate plotted against solar constant (%) in S-series simulations. In (**b**), in addition to actual pressure (*gray solid circles*), their changes from Control is decomposed into those calculated from difference in the distribution of dissolved carbon and alkalinity (*open circles*), SST (*cross*), and SSS (*triangles*). In (**d**), weathering rate is normalized by that of Control

Figure 7b displays distribution of dissolved carbon concentration in S92.3. The simulated pattern seems very similar to that of salinity (Fig. 4d). This is because diluting/condensation by freshwater flux primarily determines the distribution of dissolved carbon concentration in S92.3, which is also true for alkalinity (figure not shown). However, this diluting effect is very small for determining pCO_2 and tends to slightly decrease pCO_2 in the same way as SSS changes (e.g., Sarmient and Gruber 2006), and cannot explain the results illustrated by open circles in Fig. 6b. Because an influence of diluting/condensation by surface freshwater flux is common among all the tracer concentrations, this effect can be removed by normalizing tracer concentration using salinity,

$$C^{\circ} = C\frac{S_{ref}}{S}, \tag{4}$$

where C is a tracer concentration, and C° is a normalized concentration to reference salinity S_{ref}. Figure 7c, d displays normalized dissolved carbon and alkalinity concentrations in S92.3 in the form of difference from Control. The figures indicate that both concentrations decrease at shallow depth and increase at deep depth. This is explained by changes in the ocean circulation (Fig. 3): disappearance of northern deep water formation significantly reduces tracer exchange between the deep and surface ocean in S92.3. When we look into the figures more closely, we found that decrease of surface alkalinity is somewhat larger than that of dissolved carbon, which leads to the increase of pCO_2 (shown as open circles in Fig. 6b). Dissolved carbon changes through the budget of both organic matter and calcium carbonate, whereas alkalinity is affected mainly by the budget of calcium carbonate. Since calcium carbonate dissolves at deeper depth than organic matter, upward transport of alkalinity from the deep ocean to the surface ocean appears more strongly dependent on deep ocean circulation than that of dissolved carbon. Then, disappearance of the Atlantic deep circulation may cause larger decline of surface alkalinity than that of dissolved carbon.

It should be noted that the biological pump can also affect distribution of dissolved carbon and alkalinity. Figure 6c indicates that the export production decreases as the solar constant becomes smaller. This is explained by reduction of surface phosphate concentration whose behaviors are basically similar to those of dissolved carbon (not shown). Although the Ekman upwelling increases (Fig. 1d) and tends to enhance nutrient supply to surface, this effect is not strong enough to overcome the above-mentioned decreasing trend. The weakening of the biological pump tends to increase dissolved carbon and alkalinity at surface, then causes opposite anomaly to Fig. 7c, d. This means that the effects of changes in the biological pump are secondary to those of dilution by freshwater flux and changes in ocean circulation for explaining changes in dissolved carbon and alkalinity of Fig. 7c, d.

In summary, in the cold climate induced by reduction of the solar constant, the decrease of atmospheric CO_2 concentration as a response of the atmosphere–ocean system is resulted mainly from increased oceanic solubility of CO_2.

4.2 The C-series experiment

Next, we conduct the C-series simulations where the total carbon amount in the atmosphere–ocean system is reduced. Simulations are carried out under both 100 and 94% of the present-day solar constant. Figure 8 summaries results of this experiment. The globally ice-covered state is resulted when the total carbon amount decreases to 70 and 92% of Control for 100 and 94% of the present-day solar constant, respectively. The critical level of pCO_2 toward a globally ice-covered state is estimated around 12 and 86 ppm for 100 and 94% solar constants, respectively. The value of 86 ppm obtained here is roughly the same result as the previous studies (e.g., 100 ppm by AGCM in Jenkins and Smith 1999; 89 ppm of supercontinent case by intermediate climate model in Donnadieu et al. 2004a). This may imply that the inclusion of ocean dynamics does not affect the critical CO_2 level so seriously. The overall results obtained in this experiment are similar to those in the S-series experiment except that cooling is caused not by

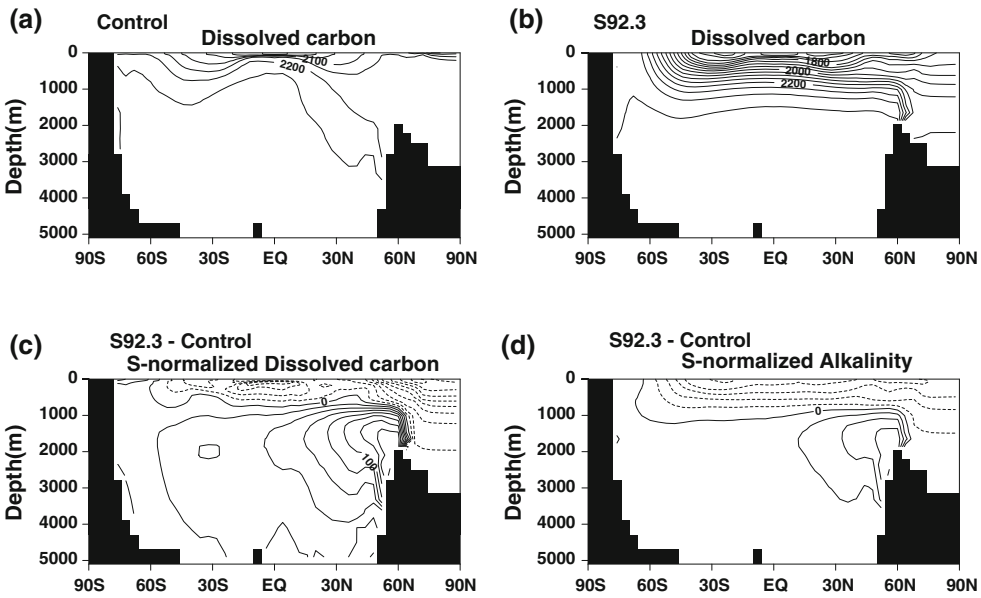

Fig. 7 Zonally averaged dissolved carbon concentration in (**a**) Control and (**b**) S92.3. Zonally averaged difference between S92.3 and Control in concentration of (**c**) dissolved carbon and (**d**) alkalinity normalized to a salinity of 35 permil. The contour interval is 50 mmol/m^3 in (**a**, **b**), and 20 mmol/m^3 in (**c**, **d**)

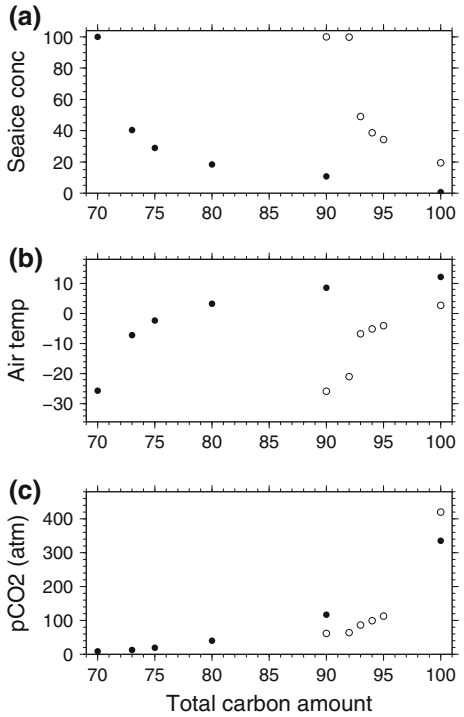

Fig. 8 The globally averaged (**a**) sea ice concentration (%), (**b**) air temperature (°C), and (**c**) atmospheric CO_2 pressure (ppm) plotted against total carbon amount (%). The *solid* and *open circles* are for C-series simulations under 100 and 94% of the present-day solar constant, respectively

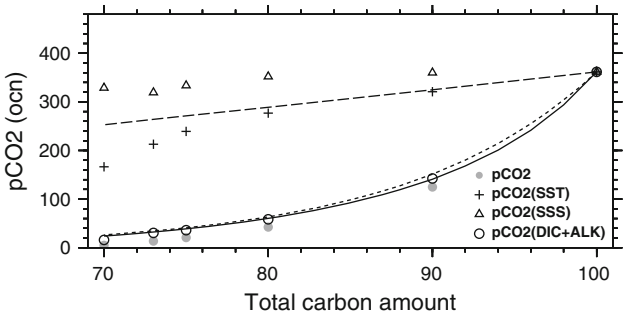

Fig. 9 Same as Fig. 6b except for C-series simulations under 100% of the present-day solar constant. Dashed line indicates atmospheric CO_2 pressure calculated by assuming a linear decrease in atmospheric CO_2 pressure proportional to total carbon amount from Control. *Dotted lines* is drawn by using the theoretical relationship of Goodwin et al. (2007) given in Eq. (6). *Solid lines* represents changes in pCO_2 obtained by explicitly calculating the response of the inorganic chemistry of oceanic carbon (see text)

reduction of the solar constant but by a decrease of the total carbon amount in the atmosphere–ocean system.

Although it is obvious that atmospheric pCO_2 decreases when total amount of carbon in the atmosphere–ocean system is reduced, its decreasing rate could be affected by various feedbacks in ocean physical and biogeochemical processes. To clarify the feedbacks, we analyze contribution of SST, SSS, dissolved carbon, and alkalinity changes for the decrease of the ocean surface pCO_2 in the C-series experiment for the present-day solar constant (Fig. 9). Contrary to the S-series experiment (Fig. 6b), changes in dissolved carbon and alkalinity primarily control pCO_2 changes. This seems obvious considering that total amount of carbon is reduced in the C-series experiment. However, it should be noted that reduction of pCO_2 is significantly larger than that expected from changes in the total carbon amount; 10% reduction of the total carbon amount (i.e., from 100 to 90% in Fig. 9) leads to more than 60% reduction of pCO_2 (i.e., from 360 to 125 ppm). This is explained by the intrinsic feature of the inorganic chemistry of oceanic carbon, which is described below.

Because most portion of carbon in the atmosphere–ocean system exists in the ocean, dissolved inorganic carbon concentration (DIC, hereafter) in the ocean changes almost linearly with the total carbon amount in the atmosphere–ocean system. The DIC is defined as the sum of oceanic carbon dioxide (pCO_2), bicarbonate iron ($[H_2CO_3^{-1}]$), and carbonate iron ($[CO_3^{-2}]$) concentrations. The inorganic chemistry of oceanic carbon controls the partition of DIC into these components. Since the oceanic pCO_2 is related to $[CO_2]$ rather than DIC, the response of the inorganic chemistry of oceanic carbon against change in the total carbon amount is very important for controlling pCO_2. The solid line in Fig. 9 indicates changes in pCO_2 explicitly calculated from the inorganic chemistry of oceanic carbon described above. Therein, we assume that DIC changes linearly with the total carbon amount and other variables (i.e., SST, SSS, and alkalinity) are unchanged from those at 100% of the total carbon amount. The figure clearly shows nonlinear behaviors of pCO_2 against the reduction of the total carbon amount, which comes from the oceanic carbon chemistry described above. The Revelle factor (ζ) is useful for describing the response of the inorganic chemistry of oceanic carbon to changes in DIC. This is defined by fractional change in pCO_2 ($\Delta pCO_2/pCO_2$) divided by that in DIC ($\Delta DIC/DIC$),

$$\zeta = \frac{\Delta pCO_2/pCO_2}{\Delta DIC/DIC}. \tag{5}$$

By using the reference value of the Revelle factor (and without explicit numerical calculation of the oceanic carbon system), Goodwin et al. (2007) provided a theory for the relation between the total carbon amount change ($\Delta(I_A + I_O)$) and ΔpCO_2;

$$\frac{pCO_2 + \Delta pCO_2}{pCO_2} = exp\left(\frac{\Delta(I_A + I_O)}{I_A + I_O/\zeta}\right), \tag{6}$$

where I_A and I_O are carbon inventory in the atmosphere and the ocean, respectively. Although Eq. (5) is applicable to small ΔpCO_2 and ΔDIC, Goodwin et al. (2007)

demonstrated that the relationship of (6) holds valid for a large change in $\Delta(I_A + I_O)$. In fact, Eq. (6) explains non-linear response of the oceanic carbon chemistry in our result very well (as shown by dotted line in Fig. 9).

In summary, it is demonstrated that the effects of changes in dissolved carbon and alkalinity on pCO_2 (as depicted by open circle in Fig. 9) are derived by the response of the inorganic chemistry of oceanic carbon to decreased DIC, and other effects such as changes in spatial distribution of dissolved carbon are negligible. In the S-series experiment, the SST effect is dominant for explaining pCO_2 changes. The SST effect has also a significant impact on pCO_2 in the C-series experiment if the total carbon amount is unchanged (as shown by cross in Fig. 9). However, when the total carbon amount decreases, the above-mentioned chemical response of oceanic carbon (solid line in Fig. 9) dominates changes in pCO_2 (grey dot in Fig. 9) and the SST effect becomes minor.

5 Discussion

5.1 Budget of total carbon amount in the atmosphere–ocean system

Results from the S-series experiment suggest that oceanic solubility of CO_2 increases in colder climate, which tends to reduce atmospheric CO_2 concentration. This suggests that ocean biogeochemical response acts as a positive feedback against climate changes to a colder state. However, the results obtained from the C-series experiment indicate that atmospheric CO_2 concentration is controlled mainly by degrees of reduction of the total carbon amount in the atmosphere–ocean system, rather than changes in oceanic solubility of CO_2. If cold climate is induced by the reduction of atmospheric CO_2 concentration due to reduction of the total carbon amount, it is important to reveal how the biogeochemical response of the ocean affects the budget of the total carbon amount in the atmosphere–ocean system. The total carbon amount in the atmosphere–ocean system (M_{AO}) varies on timescale of 10^5 years as described below. It is determined under the balance among fluxes due to outgas of mantle CO_2 via volcanism (F_V), degassing of CO_2 via metamorphism-volcanism at subduction zone (F_M), weathering (F_W), and burial (F_B):

$$\frac{dM_{AO}}{dt} = F_V + F_M + F_W^O + F_W^C - F_B^O - F_B^C, \tag{7}$$

where subscripts O and C represent organic and carbonate carbon, respectively (e.g., Walker et al. 1981; Tajika 2003). If we assume the mass balance of calcium iron in the ocean is in a steady state, the following equation is obtained (e.g., Berner 1994),

$$F_B^C - F_W^C = F_W^S, \tag{8}$$

where F_W^S represents the silicate weathering followed by carbonate precipitation in the ocean. From the above relationship, Eq. (7) becomes

$$\frac{dM_{AO}}{dt} = F_D + F_W^O - F_B^O - F_W^S, \tag{9}$$

where F_D is total degassing rate of CO_2 (i.e., $F_V + F_M$). The terms F_D and F_W^O are inflowing carbon flux into the atmosphere–ocean system, and the terms F_B^O and F_W^S are the outflowing carbon flux.

Following Calderia and Kasting (1992), F_W^S is roughly estimated by:

$$F_W^S = F_{W0}^S \left(\frac{P-E}{P_0-E_0}\right)^{0.5} exp\left(\frac{T-T_0}{13.7K}\right), \tag{10}$$

where T is globally averaged air temperature, $P - E$ is globally averaged precipitation minus evaporation over land (which is assumed to be proportional to fresh soil water here), and the subscript 0 refers to the present-day value. Figure 6d displays F_W^S estimated in the S-series simulations. The figure suggests that F_W^S decreases as the climate becomes colder since T (Fig. 1b) and $P - E$ (Fig. 1c) decreases. As a consequence, F_W^S becomes 10% of Control just before the global glaciations. As for F_B^O, it is determined from the amount of carbon flux at seafloor and dissolution process within the ocean sediment. Because the carbon flux at seafloor is strongly dependent on the export flux of organic carbon from the surface ocean, we can roughly estimate change in F_B^O from the export production. Figure 6c suggests that F_B^O also decreases in colder climate and becomes 70% of Control just before the global glaciations. Therefore, both F_W^S and F_B^O should decrease in colder climate. This means that outgoing carbon flux from the atmosphere–ocean system decreases, resulting in accumulation of M_{AO} and increase in atmospheric CO_2 concentration, if F_D and F_W^O remain constant. The processes of carbon consumption are therefore expected to act as a negative feedback mechanisms against the climate cooling caused by decrease in the total carbon amount of atmosphere–ocean system. Because the atmospheric CO_2 pressure strongly depends on the total carbon amount rather than oceanic solubility of CO_2 (Fig. 9), this feedback is significantly stronger than a positive feedback of oceanic solubility identified in S-series simulations.

Here, we discuss possible mechanisms which cause the reduction of atmospheric CO_2 concentration and trigger the global glaciations. As we already discussed, F_W^S and F_B^O are expected to become significantly lower as the climate becomes colder at least under the present land-sea distribution. This means that the response plays a negative feedback, against the decrease of the total carbon amount,

and tends to prevent from being the global glaciated. Therefore, if other factors do not affect (9), the possible mechanism for reducing the total carbon amount would be decrease of F_D, that is, reduction of total degassing rate of CO_2 since this is determined independently from the feedback loop of the atmosphere–ocean system.

The timescale of the Earth to become globally glaciated can be roughly estimated from the total amount of carbon in the atmosphere–ocean system and pCO_2 flux into/out of the system. At present, 597 Gt and 38,000 Gt of carbon is stored in the atmosphere and the ocean, respectively (Denman et al. 2007), and F_D is estimated to be 9.4×10^{-2} Gt C/year (Berner 1991). The time required for achieving a globally ice-covered state by the reduction of the total carbon amount is on the order of 10^5 years. The feedback effects (decrease of F_W^S and F_B^O) tend to prolong this estimate to some degrees. Therefore, halting of volcanic pCO_2 degassing on the order of 10^5 years may result in global glaciations for the present Earth.

5.2 Implication for the Neoproterozoic snowball earth events

We have investigated how the ocean circulation and ocean carbon cycle change if the solar constant or the total carbon amount is reduced from the present Earth conditions. The results may be different in several aspects from the actual climate changes that occurred during the Neoproterozoic. For example, continental distribution during the Neoproterozoic was completely different from that at present, which is a very important boundary condition for the ocean. We showed that the ocean thermohaline circulation changes from thermally driven circulation to salinity-driven circulation in the course of global glaciations. We believe that this is also applicable for the Neoproterozoic snowball earth events. On the other hand, our result suggests that the deep ocean is ventilated exclusively by deep water formation in the southern high latitudes just before the global glaciations, which should depend on the continental distribution. This result is derived from the fact that the sea ice is more massively transported in the southern hemisphere than in the northern hemisphere under the present-day continental distribution (because there is less land in southern hemisphere). During the Neoproterozoic, almost all the continents located in low and middle latitudes, and sea ice is transported more equally between northern and southern hemispheres than today. It is implied that subtle difference in the land-sea distribution between northern and southern hemispheres could affect the ocean thermohaline circulation at that time. The break-up of the supercontinent Rodinia may have occurred at around 750 Ma, and the Sturtian glaciations is considered to have taken place after that. We need to know more exact knowledge about timing of snowball earth events and the continental distribution, which will be helpful for simulating the ocean circulation at that time more accurately.

We also demonstrate that the atmosphere–ocean system has strong negative feedback loops against decline of the total carbon content, and it is also implied that global glaciations could be caused by the processes outside the atmosphere–ocean feedback loops. We believe this is applicable to the Neoproterozoic snowball earth events. In the discussion, if the present Earth becomes globally glaciated, we further speculate that the long-term suppression of volcanic pCO_2 degassing rate may be a possible mechanism. As for the Neoproterozoic glaciations, there is no direct evidence for the volcanic activities although some studies suggest the possibility of changes in the pCO_2 degassing rate (Tajika 2004; Santosh and Omori 2008). We therefore do not rule out other possibilities which might have caused the Neoproterozoic snowball earth events, because processes not considered in our simulations may have been important for the Neoproterozoic glaciations. Donnadieu et al. (2004a, b proposed that, in addition to an increase in precipitation and runoff due to the break-up of the supercontinent Rodinia, the basaltic provinces formed by eruption of the super-plume which caused the break-up of Rodinia could have enhanced an efficiency of silicate weathering, resulting in the global glaciations. Investigation into the cause of Neoproterozoic snowball earth events is beyond our scope of this study, and needs to be discussed in future.

6 Summary

In order to investigate changes of ocean circulation and ocean carbon cycle through the course of global glaciations from the present Earth, we conducted a series of simulations by reducing the solar constant from the present value in the systematic way (S-series experiment). When the climate approaches a globally ice-covered state, we found that the thermohaline circulation is driven by the surface freshwater forcing since the surface heat flux almost vanishes by the sea-ice insulation effect. The ocean biogeochemical cycle considered in this model is more sophisticated than those used in the previous studies. We identified that the most important process affecting the atmospheric pCO_2 is an increase of oceanic solubility associated with SST change. Although this solubility effect itself is well known, we clearly demonstrated that this becomes dominant among other processes (e.g., changes in biological pump, redistribution of DIC and alkalinity by ocean circulation) in S-series experiment.

We then performed a series of simulations by reducing the total amount of carbon in the atmosphere and ocean

system (C-series experiment). Under 94% of the present solar constant, the Earth becomes globally glaciated when the total carbon amount becomes less than 70% of the present amount. The critical level of atmospheric pCO_2 at that condition is estimated to be 86 ppm. In C-series experiment, the atmospheric pCO_2 is strongly controlled by the total carbon amount, which overcomes the oceanic solubility effect identified in S-series experiment. This means that investigation into the processes which control the total carbon amount is essential for explaining changes in the atmospheric pCO_2 in the course of global glaciations.

We also discussed the processes controlling the total carbon amount. By using results from S-series and C-series experiments, we investigated what kind of feedbacks affect the total carbon amount in atmosphere and ocean system. We found that the silicate weathering and ocean burial of organic carbon become smaller at colder climate and they act as strong negative feedbacks toward global glaciations. This implies that global glaciations may have been caused by processes outside the atmosphere–ocean feedback loops. A large reduction of volcanic CO_2 degassing on the order of 10^5 years, for example, could reduce the atmospheric pCO_2.

Because we focused on a transitional process to global glaciations from the present Earth conditions, our simulation of global glaciations may be different in several aspects from the Neoproterozoic snowball earth events. However, we may obtain the robust results which are also applicable to the Neoproterozoic snowball earth events. In the course of global glaciations, we show that the ocean thermohaline circulation becomes driven by sea ice forming/melting. In addition, we demonstrated that the atmosphere–ocean system has strong negative feedback loops against decline of the total carbon content. The latter result implies that global glaciations may be caused by the processes outside the atmosphere–ocean feedback loops such as long-term suppression of volcanic CO_2 degassing rate. While the cause for the Neoproterozoic snowball Earth events has been unknown, this might have been one of possibilities in addition to a possibility of increased silicate weathering rate due to the break-up of a supercontinent Rodinia.

Acknowledgments The authors greatly appreciate useful comments by anonymous reviewers. The model calculations were performed by HITACHI SR11000 at Information Technology Center, University of Tokyo. The figures were produced by using the Dennou Library (developed by the GFD-Dennou Club) and GMT.

Appendix

In the Appendix, we describe details of atmosphere and land components of MIROC-lite. The ocean biogeochemical model is also described in detail here.

MIROC-lite model description

The prognostic variables are air temperature (T_a) and air specific humidity (q_a) for the atmosphere model, and ground temperature (T_g), ground water content (w_g), and ground snow amount (s_g) for the land model.

Atmosphere model

The model predicts T_a by solving the vertically integrated energy balance equation (Oka et al. 2001).

$$C_a\frac{\partial T_a}{\partial t} = Q_{sw} - Q_{lw} + Q_t - Q_{sfc}, \tag{11}$$

where C_a is the heat capacity of the air column, t is time, Q_{sw} and Q_{lw} are the net incoming shortwave and outgoing longwave radiation at the top of the atmosphere, Q_t is the convergence of the horizontal heat transport by the atmosphere, and Q_{sfc} is the net downward heat flux at the sea or land surface.

The net incoming shortwave radiation is expressed by

$$Q_{sw} = S_{in} - S_{out}, \tag{12}$$

where S_{in} and S_{out} are the incoming and outgoing shortwave radiation at the top of the atmosphere, respectively. S_{in} is calculated from the solar constant and earth's orbital parameters (Berger 1978). The atmospheric reflection coefficient (C_{sr}), absorption coefficient (C_{sa}), and surface albedo (α_s) determine S_{out};

$$S_{out} = C_{sr}S_{in} + (1 - C_{sr} - C_{sa})^2\alpha_s(1 + \alpha_s C_{sr} + \alpha_s^2 C_{sr}^2 + ...)S_{in} \tag{13}$$

$$= C_{sr}S_{in} + (1 - C_{sr} - C_{sa})^2\frac{\alpha_s}{1 - \alpha_s C_{sr}}S_{in}, \tag{14}$$

where the second term in the right-hand side represents contribution from multiply-scattered shortwave radiation. C_{sr} and C_{ca} are the function of latitude (θ);

$$C_{sr} = 0.607187 - 0.3862120cos\theta, \tag{15}$$

and

$$C_{sa} = 0.103834 + 0.0751783cos\theta. \tag{16}$$

They are empirically determined so that S_{out} (and S_{sfc}, see below) becomes similar to that of the present climate. The surface albedo depends on surface type (prescribed as boundary condition) and snow amount.

As in traditional EBMs, Q_{lw} is parameterized by a linear function of surface air temperature (T_s);

$$Q_{lw} = A + BT_s, \tag{17}$$

and T_s is calculated from T_a by assuming constant lapse rate of the atmosphere (Γ);

$$T_s = T_a - \Gamma z_{sfc}, \tag{18}$$

where z_{sfc} is elevation of land above sea level prescribed as boundary condition. While A and B are constant in S-series experiment, they are determined from atmospheric pCO_2 in C-series experiment with the formulation of Caldeira and Kasting (1992a, b).

The heat transport of the atmosphere is parameterized in the form of the diffusion;

$$Q_t = C_a \nabla \cdot (\kappa \nabla T_a), \tag{19}$$

where κ is the heat diffusion coefficient.

The surface flux consists of the net downward shortwave flux (S_{sfc}), the upward (Q_{lu}) and downward (Q_{ld}) longwave fluxes, and sensible (Q_{sh}) and latent (Q_{lh}) heat fluxes at the surface;

$$Q_{sfc} = S_{sfc} - (Q_{lu} - Q_{ld}) - Q_{sh} - Q_{lh}. \tag{20}$$

As in (14), S_{sfc} is represented by

$$S_{sfc} = (1 - C_{sr} - C_{sa})(1 + \alpha_s C_{sr} + \alpha_s^2 C_{sr}^2 + ...)(1 - \alpha_s) S_{in} \tag{21}$$

$$= (1 - C_{sr} - C_{sa}) \frac{1 - \alpha_s}{1 - \alpha_s C_{sr}} S_{in}. \tag{22}$$

The upward longwave flux is represented in the form of linear expansion of Boltzmann's law,

$$Q_{lu} = A_u + B_u T_{sfc}, \tag{23}$$

where A_u and B_u are constant values and T_{sfc} is surface temperature. In the case of no snow, T_{sfc} corresponds to SST over ocean and T_g over land. If a model grid is totally covered with snow, T_{sfc} corresponds to snow top temperature, and in this case, T_{sfc} is determined as a result of heat budget calculation within snow layer. Since a grid can be partially covered with snow, we introduce two variables T_{sfc1} (surface temperature over snow-free area) and T_{sfc2} (snow top temperature), and T_{sfc} is defined by

$$T_{sfc} = (1 - A_{snow}) T_{sfc1} + A_{snow} T_{sfc2}, \tag{24}$$

where A_{snow} is the fraction of area covered with snow. The surface coverage of snow is parameterized by

$$A_{snow} = \sqrt{\frac{s_g}{s_{max}}}, \tag{25}$$

where s_{max} is maximum snow amount.

In the same way as Q_{lu}, the downward longwave radiation is represented by

$$Q_{ld} = A_d + B_d T_s, \tag{26}$$

where A_d and B_d are constant values.

The sensible heat flux is calculated from bulk formulae;

$$Q_{sh} = U_{sfc} C_H \rho C_P (T_{sfc} - T_s), \tag{27}$$

where U_{sfc} is the surface wind speed, C_H is the bulk coefficient for the sensible heat flux, ρ is the air density, and C_P is the heat capacity of air.

The latent heat flux comes from water evaporation (W_{evap}) and snow sublimation (W_{subl});

$$Q_{lh} = L_v W_{evap} + (L_V + L_M) W_{subl}, \tag{28}$$

where L_V and L_M are latent heat of evaporation and melting, respectively. The expression of W_{evap} and W_{subl} will be described later.

The prognostic equation of the air specific humidity is

$$C_w \frac{\partial q_a}{\partial t} = W_{evap} + W_{subl} - W_P + W_T, \tag{29}$$

where C_w is a parameter controlling vertically integrated atmospheric water content, W_P is precipitation, and W_T is the convergence of the atmospheric water transport. By assuming sub-grid distribution of q_a where air specific humidity distributes homogeneously between $(1 - b)q_a$ and $(1 + b)q_a$, the precipitation is parameterized by

$$W_P = \begin{cases} 0 & (1+b)q_a \le q_{sat}(T_a) \\ \frac{(1+b)q_a - q_{sat}(T_a)}{4bq_a \Delta t} & (1-b)q_a < q_{sat}(T_a) < (1+b)q_a \\ \frac{q_a - q_{sat}(T_a)}{\Delta t} & (1-b)q_a \ge q_{sat}(T_a), \end{cases} \tag{30}$$

where q_{sat} is the saturation specific humidity, and b is a parameter controlling sub-grid distribution of q_a.

From bulk formulae, W_{evap} is calculated by

$$W_{evap} = U_{sfc} C_E \rho \beta (q_{sat}(T_{sfc}) - q_s)(1 - A_{snow}), \tag{31}$$

where C_E is the bulk coefficient for the latent heat flux, β is evaporation efficiency, and q_s is surface air specific humidity. In a manner analogous to (18), q_s is estimated as

$$q_s = q_a \frac{q_{sat}(T_s)}{q_{sat}(T_a)}. \tag{32}$$

The evaporation efficiency is a function of ground water content;

$$\beta = \begin{cases} 1 & (ocean) \\ \frac{W}{W_{crt}} & (land), \end{cases} \tag{33}$$

where W is saturation fraction of ground water and W_{crt} is its critical value. The saturation fraction is expressed by

$$W = \frac{w_g}{w_{max}}, \tag{34}$$

where w_{max} is maximum water content of land (i.e., bucket capacity of the land model).

As in W_{evap}, W_{subl} is calculated by

$$W_{subl} = U_{sfc} C_E \rho (q_{sat}(T_{sfc}) - q_s) A_{snow}. \tag{35}$$

The atmospheric vapor transport consists of advection and diffusion terms;

$$W_T = C_w \nabla (q_a \mathbf{v} - K_Q \nabla q_a), \tag{36}$$

where $\mathbf{v}$ is atmospheric wind, and K_Q is diffusion coefficient. As described in Oka et al. (2001), $\mathbf{v}$ is diagnosed from T_a. The model also has an option where $\mathbf{v}$ is prescribed from externally specified distribution in the same way as Weaver et al. (2001).

Land model

As a land model, one layer bucket model is included in the model and the ground temperature is calculated by

$$C_g \frac{\partial T_g}{\partial t} = Q_{sfc} - Q_{melt}, \tag{37}$$

where C_g is heat capacity of land, and Q_{melt} represents latent heat release by snow melting. In case that T_{sfc2} exceeds freezing point (T_{ice}) as a result of heat budget calculation, Q_{melt} becomes a non-zero value;

$$Q_{melt} = \begin{cases} C_g (T_{sfc2} - T_{ice}) A_{snow} & T_{sfc2} > T_{ice} \text{ and } w_s > 0 \\ 0 & elsewhere. \end{cases} \tag{38}$$

The ground water content is calculated by

$$C_{wg} \frac{\partial w_g}{\partial t} = W_{rain} - W_{evap} + W_{melt} - W_{roff}, \tag{39}$$

where C_{wg} is water capacity of land, W_{rain} is rainfall, W_{melt} is melting rate of snow, and W_{roff} is river runoff. Note that W_P consists of two components: rainfall (W_{rain}) and snowfall (W_{snow}). The separation of these components is parameterized by

$$W_{snow} = \begin{cases} 0 & T_s \geq T_{rain} \\ \frac{T_s - T_{snow}}{T_{rain} - T_{snow}} W_P & T_{snow} < T_s < T_{rain} \\ W_P & T_s \leq T_{snow}, \end{cases} \tag{40}$$

$$W_{rain} = W_P - W_{snow}, \tag{41}$$

where T_{rain} and T_{snow} are parameters determining separation between rainfall and snowfall.

As for W_{melt}, it is equivalent to Q_{melt};

$$W_{melt} = \frac{Q_{melt}}{L_M}. \tag{42}$$

The amount of water which exceeds the critical value is transported into the ocean as the river runoff,

$$W_{roff} = \begin{cases} \frac{w_g - w_{max}}{\Delta t} & w_g > w_{\max} \\ 0 & w_g \leq w_{max}. \end{cases} \tag{43}$$

To close the water budget, W_{roff} of each land model grid is redistributed over the whole ocean grids homogeneously in this study. The model has an option where W_{roff} is transported into the ocean following river route given as boundary condition.

The snow amount is calculated by

$$\frac{\partial s_g}{\partial t} = W_{snow} - W_{subl} - W_{melt} - W_{soff}, \tag{44}$$

where W_{soff} is snow flux entering into the ocean. As in W_{roff}, the amount of snow which exceeds the critical value is discharged into the ocean,

$$W_{soff} = \begin{cases} \frac{s_g - s_{max}}{\Delta t} & s_g > s_{max} \\ 0 & s_g < s_{max}. \end{cases} \tag{45}$$

Ocean biogeochemical model description

The model is based on Yamanaka and Tajika (1996) where concentrations of phosphate (P), dissolved inorganic carbon (DIC), and alkalinity (ALK) are calculated as prognostic variables. The concentration of these variables is determined from the following equation:

$$\frac{\partial C}{\partial t} = -v \cdot \nabla C + K_H \nabla_H^2 P + K_V \frac{\partial^2 C}{\partial^2 z} + S_C, \tag{46}$$

where C is concentration (i.e, P or DIC or ALK), v is oceanic velocity, K_H and K_V are respectively horizontal and vertical diffusivity, and S_C is a source/sink term associated with biogeochemical processes. Note that the isopycnal and layer thickness diffusions are not explicitly written in (46) but actually included in the model calculation. The velocity and diffusion coefficients in (46) are given from the OGCM, and the source/sink terms for P, DIC, ALK are described below.

Firstly, the source/sink term of phosphate (S_P) is expressed by

$$S_P = -\Gamma + \frac{dF}{dz}, \tag{47}$$

where Γ is uptake rate of phosphate, F is downward flux of particulate organic phosphate, and z is depth (positive for downward). Γ is diagnosed from in situ phosphate concentration:

$$\Gamma = \begin{cases} r L_f P \frac{P}{h+P} & (z < z_e) \\ 0 & (z \geq z_e), \end{cases} \tag{48}$$

where z_e is depth of euphotic zone, r is maximum uptake ratio, L_f is light factor (a simple function of latitude and normalized to be $0 < L_f < 1$), and h is a half saturation constant. The export production (EP) is determined from vertical integral of (48) within the euphotic zone;

$$EP = \int_0^{z_e} \Gamma dz. \tag{49}$$

By using EP, F is represented by a power law obtained from sediment traps (Martin et al. 1987).

$$F = \begin{cases} EP & (z < z_e) \\ EP \left(\frac{z}{z_e}\right)^{-0.858} & (z \geq z_e). \end{cases} \tag{50}$$

Secondly, the source/sink term of alkalinity (S_{ALK}) is expressed by

$$S_{ALK} = R_{PN}S_P - 2(-R_{rain}R_{PC}\Gamma + \frac{dF_{CaCO3}}{dz}), \quad (51)$$

where R_{PN} (R_{PC}) is the Redfield ratio between phosphate and nitrate (carbon), R_{rain} is a ratio of production rate of calcium carbonate to that of particulate organic carbon, and F_{CaCO3} is vertical flux of calcium carbonate. The profile of calcium carbonate is taken from the control case of Yamanaka and Tajika (1996);

$$F_{CaCO3} = \begin{cases} F_0 & (z < z_e) \\ F_0 exp(-\frac{z-z_e}{3{,}500\,m}) & (z \geq z_e), \end{cases} \quad (52)$$

where F_0 is vertical flux of calcium carbonate at the bottom of the euphotic zone;

$$F_0 = \int_0^{z_e} R_{rain}R_{PC}\Gamma dz. \quad (53)$$

Finally, the source/sink term of total dissolved carbon (S_{DIC}) is expressed by

$$S_{DIC} = R_{PC}S_P + (-R_{rain}R_{PC}\Gamma + \frac{dF_{CaCO3}}{dz}) + S_{gas}. \quad (54)$$

The last term (S_{gas}) represents gas exchange between the ocean and the atmosphere:

$$S_{gas} = \begin{cases} \frac{K_W \alpha}{\Delta z}(pCO_2|_{atm} - pCO_2|_{ocn})(1 - A_{ice}) & (z < \Delta z) \\ 0 & (z > \Delta z), \end{cases} \quad (55)$$

where K_W is piston velocity, α is solubility, Δz is thickness of model top layer, $pCO_2|_{atm}$ and $pCO_2|_{ocn}$ is respectively atmosphere and ocean partial pressure of CO_2, and A_{ice} is fraction of sea ice. Based on inorganic chemistry of carbon system, the ocean partial pressure ($pCO_2|_{ocn}$) is determined from sea surface *DIC*, sea surface *ALK*, SST, and SSS; this is symbolically expressed as

$$pCO_2|_{ocn} = f(DIC, ALK, SST, SSS), \quad (56)$$

where f represents a function determined from inorganic chemistry of carbon system. The model includes a well-mixed atmosphere box in which atmospheric CO_2 concentration (i.e., $pCO_2|_{atm}$) is calculated from gas exchange between the ocean and the atmosphere.

References

Baum SK, Crowley TJ (2001) GCM response to Late Precambrian (590 Ma) ice-covered continets. Geophys Res Lett 28:583–586

Berger AL (1978) Long-term variations of caloric insolation resulting from the Earth's orbital elements. Quaternary Res 9:139–167

Berner RA (1991) A model for atmospheric CO_2 over Phanerozoic time. Am J Sci 291:339–376

Berner RA (1994) GEOCARB II: a revised model of atmospheric CO_2 over Phanerozoic time. Am J Sci 294:56–91

Budyko MI (1969) The effect of solar radiation variations on the climate of the earth. Tellus 21:611–619

Caldeira K, Kasting JF (1992) Susceptibility of the early Earth to irreversible glaciation caused by carbon dioxide clouds. Nature 359:226–228

Caldeira K, Kasting JF (1992) The life span of the biosphere revisited. Nature 360:721–723

Chandler MA, Sohl LE (2000) Climate forcings and the initiation of lowlatitude ice sheets during the Neoproterozoic Varanger glacial interval. J Geophys Res 105:20737–20756

Conkright M, Garcia H, O'Brien T, Locarnini R, Boyer T, Stephens C, Antonov J (2002) NOAA Atlas NESDIS 21: World Ocean Atlas 2001, Nutrients, vol 1. Silver Sprint, MD, 392pp

Cox MD (1987) Isopycnal diffusion in a z-coordinate ocean model. Ocean Model 74:1–5

Crowley TJ, Baum SK (1993) Effect of decreased solar luminosity on late Precambrian ice extent. J Geophys Res 98:16723–16732

Denman KL, Brasseur G, Chidthaisong A, Ciais P, Cox PM, Dickinson RE, Hauglustaine D, Heinze C, Holland E, Jacob D, Lohmann U, Ramachandran S, da Silva Dias PL, Wofsy SC, Zhang X (2007) Couplings between changes in the climate system and biogeochemistry. In: Solomon S, Qin D, Manning M, Chen Z, Marquis M, Averyt KB, Tignor M, Miller HL (eds) Climate change 2007: the physical science basis. Contribution of working group I to the fourth assessment report of the intergovernmental panel on climate change, Cambridge University Press, Cambridge

Donnadieu Y, Godderis Y, Ramstein G, Nedelec A, Meert J (2004a) A 'snowball Earth' climate triggered by continental break-up through changes in runoff. Nature 428:303–306

Donnadieu Y, Ramstein G, Fluteau F, Roche D, Ganopolski A (2004b) The impact of atmospheric and oceanic heat transports on the sea-ice-albedo instability during the Neoproterozoic. Clim Dyn 22:293–306

Evans D (2000) Stratigraphic, geochronological, and paleomagnetic constraints upon the Neo-proterozoic climatic paradox. Am J Sci 300:347–433

Gent PR, Willebrand J, McDougall TJ, McWilliams James C (1995) Parameterizing eddy-induced tracer transports in ocean circulation models. J Phys Oceanogr 25:463–474

Goodman JC, Pierrehumbert RT (2003) Glacial flow of floating marine ice in "Snowball Earth". J Geophys Res 108. doi: 10.1029/2002JC001471

Goodwin P, Williams RG, Follows MJ, Dutkiewicz S (2007) Oceanatmosphere partitioning of anthropogenic carbon dioxide on centennial timescales. Glob Biogeochem Cycles 21. doi: 10.1029/2006GB002810

Gough DO (1981) Solar interior structure and luminosity variations. Solar Phys 74:21–34

Hoffman PF, Kaufman AJ, Halverson GP, Schrag DP (1998) A Neoproterozoic Snowball Earth. Science 28:1342–1346

Hoffman PF, Schrag DP (2000) Snowball Earth. Sci Am 282:68–75

Hasumi H, Suginohara N (1995) Haline circulation induced by formation and melting of sea ice. J Geophys Res 100:20613–20625

Hasumi H (2006) CCSR Ocean component model (COCO) Version 4.0. CCSR report No. 25, 103 pp

Hunke EC, Dukowicz JK (1997) An elastic–viscous–plastic model for sea ice dynamics. J Phys Oceanogr 27:1849–1867

Hyde WT, Crowley TJ, Baum SK, Peltier WR (2000) Neoproterozoic 'snowball Earth' simulations with a coupled climate/ice-sheet model. Nature 405:425–429

Jenkins GS, Smith SR (1999) GCM simulations of Snowball Earth conditions during the late Proterozoic. Geophys. Res Lett 26:2263–2266

K-1 Model Developers (2004) Coupled GCM (MIROC) description. In: Hasumi H, Emori S (eds) K-1 technical report No. 1

Kaufman AJ, Knoll AH, Narbonne GM (1997) Isotopes, ice ages, and terminal Proterozoic earth history. Natl Acad Sci Proc 94:6600–6605

Key RM, Kozyr A, Sabine CL, Lee K, Wanninkhof R, Bullister JL, Feely RA, Millero FJ, Mordy C, Peng T-H (2004) A global ocean carbon climatology: results from Global Data Analysis Project (GLODAP). Glob Biogeochem Cycles 18. doi: 10.1029/2004GB002247

Killworth PD, Stainforth D, Webb DJ, Paterson SM (2003) The development of a free-suface Bryan-Cox-Semtner ocean model. J Phys Oceanogr 21:1333–1348

Komuro Y, Hasumi H (2003) Intensification of the Atlantic deep circulation by the Canadian Archipelago throughflow. J Phys Oceanogr 35:775–789

Lewis JP, Eby M, Weaver AJ, Johnston ST (2004) Global glaciation in the Neoproterozoic: reconciling previous modelling results. Geophys Res Lett 31:L08201. doi:10.1029/2004GL019725

Lewis JP, Weaver AJ, Eby M (2007) Snowball versus slushball Earth: dynamic versus nondynamic sea ice? J Geophys Res 112:C11014. doi:10.1029/2006JC004037

Martin J, Knauer G, Karl D, Broenkow W, (1987) Vertex: carbon cycling in the northeast Pacific. Deep Sea Res Part I 34:267–285

Noh Y, Kim HJ (1999) Simulation of temperature and turbulance structure of the oceanic boundary layer with the improved near-surface process. J Geophys Res 104(C7):15621–15634

North GR (1981) Energy balance climate models. Rev Geophys Space Phys 19:91–121

Oka A, Hasumi H, Suginohara N (2001) Stabilization of the thermohaline circulation by wind-driven and vertical diffusive salt transport. Clim Dyn 18:71–83

Oka A, Hasumi H, (2004) Effects of freshwater forcing on the Atlantic deep circulation: a study with an OGCM forced by two different surface freshwater flux datasets. J Clim 17:2180–2194

Peltier WR, Liu Y, Crowley JW (2007) Snowball Earth prevention by dissolved organic carbon remineralization. Nature 450. doi: 10.1038/nature06354

Poulsen CJ, Pierrehumbert RT, Jacob RL (2001) Impact of ocean dynamics on the simulation of the Neoproterozoic snowball Earth. Geophys Res Lett 28:1575–1578

Poulsen CJ, Jacob RL, Pierrehumbert RT, Huynh TT (2002) Testing paleogeographic controls on a Neoproterozoic snowball Earth. Geophys Res Lett 29. 10.1029/2001GL014352

Sarmient JL, Gruber N,(2006) Ocean biogeochemical dynamics. Princeton University Press, Princeton

Santosh M, Omori S (2008) CO_2 windows from mantle to atmosphere: models on ultrahigh-temperature metamorphism and speculations on the link with melting of snowball Earth. Gondwana Res 14:82–96

Sellers WD (1969) A climate model based on the energy balance of the earthatmosphere system. J Appl Meteor 8:392–400

Semtner AJ Jr (1976) A model for the thermodynamic growth of sea ice in numerical investigations of climate. J Phys Oceanogr 6:379–389

Steele M, Morley R, Ermold W (2001) PHC: a global ocean hydrography with a high-quality Arctic Ocean. J Clim 14:2079–2087

Tajika E (1999) Carbon cycle and climate change during the Cretaceous inferred from a carbon biogeochemical cycle model. Island Arc 8:293–303

Tajika E (2003) Fait young Sun and the carbon cycle: implication for the Proterozoic global glaciations. Earth Planet Sci Lett 214:443–453

Tajika E (2004) Analysis of carbon cycle system during the Neoproterozoic: implication for snow ball Earth events. In: Jenkins G, Mckay C, Sohl L (eds) Multidisciplinary studies exploring extreme proterozoic environment conditions, p 220. AGU Geophysical Monograph, American Gephysical Union, vol 146, pp 45–54

Tanaka Y, Hasumi H (2008) Injection of Antarctic Intermediate Water into the Atlantic subtropical gyre in an eddy resolving ocean model. Geophys Res Lett 35:L11601

Yamanaka Y, Tajika E (1996) The role of the vertical fluxes of particulate organic matter and calcite in the oceanic carbon cycle: studies using an ocean biogeochemical general circulation model. Glob Biogeochem Cycles 10:361–382

Walker JCG, Hays PB, Kasting JF (1981) A negative feedback mechanism for the long-term stabilization of Earth's surface temperature. J Geophys Res 86:9776–9782

Watanabe E, Hasumi H (2009) Pacific water transport in the western Arctic Ocean simulated by an eddy-resolving coupled sea ice-ocean model. J Phys Oceanogr 39. doi:10.1175/2009JPO4010.1

Weaver AJ, Eby M, Wiebe EC, Bitz CM, Duffy PB, Ewen TL, Fanning AF, Holland MM, MacFadyen A, Matthews HD, Meissner J, Saenko O, Schmittner A, Wang H, Yoshimori M (2001) The UVic Earth system climate model: model description, climatology, and applications to past, present and future climates. Atmos-Ocean 39: 364-428